

Article

Maximum Impacts of the Initial and Model Parametric Errors on El Niño Predictions

Lingjiang Tao 

School of Marine Sciences, Nanjing University of Information Science and Technology, Nanjing 210044, China; taolingjiang@nuist.edu.cn or taolj1992@foxmail.com

Abstract: With an El Niño prediction model, an advanced approach of conditional nonlinear optimal perturbation (CNOP) is used to reveal the maximum impacts of the errors occurring in initial conditions (ICs) and model parameters (MPs) on the El Niño predictions. The optimally growing initial errors CNOP-I and parameter errors CNOP-P are obtained, as well as their optimally combined mode (denoted by CNOPs). The comparisons among CNOP-I, -P, and CNOPs show that the El Niño predictions are more sensitive to the uncertainties in the MPs than in the ICs. The CNOP-I mainly affects the short-term prediction (less than 3 months), whereas the CNOP-P tends to induce much larger error over a longer prediction time. Both CNOP-I and CNOP-P can induce larger error growth during spring than during other seasons; that is to say, both of them cause the “spring predictability barrier” (SPB) phenomenon. The spring error growth caused by CNOP-I is mainly attributed to the uncertainties of the ocean advection processes, while that caused by the CNOP-P is controlled by thermodynamics. When the errors in ICs and MPs are simultaneously included in predictions, the resultant CNOPs produce much larger error growth and cause much more significant SPB; furthermore, the corresponding mechanism is dominated by the nonlinear advection processes. This certainly indicates that strong nonlinear interactions between the errors in ICs and MPs enhance the SPB, thus deepening our understanding of El Niño predictability. It is obvious that initial and model errors should be simultaneously given great attention to improve the El Niño prediction level.

Keywords: El Niño predictability; condition nonlinear optimal perturbation; initial uncertainties; parametric uncertainties



Citation: Tao, L. Maximum Impacts of the Initial and Model Parametric Errors on El Niño Predictions. *J. Mar. Sci. Eng.* **2024**, *12*, 601. <https://doi.org/10.3390/jmse12040601>

Academic Editor: Jean-Louis Pinault

Received: 1 March 2024

Revised: 26 March 2024

Accepted: 28 March 2024

Published: 30 March 2024



Copyright: © 2024 by the author. Licensee MDPI, Basel, Switzerland. This article is an open access article distributed under the terms and conditions of the Creative Commons Attribution (CC BY) license (<https://creativecommons.org/licenses/by/4.0/>).

1. Introduction

El Niño, characterized by anomalous warming in the eastern-central equatorial Pacific [1], has drawn great public attention for its global effect on society and the natural climate system [2–4]. As a strong air–sea coupling phenomenon in the earth system, El Niño has genes of quasi-periodicity but features of complexity, diversity, and variability [5,6]. Therefore, although efforts towards the prediction of El Niño have never been stopped [7–11], operational prediction for the sea surface temperature (SST) in the tropical Pacific is still faced with huge challenges (e.g., [12,13]).

On the one hand, the El Niño evolution is modified by the atmospheric processes with high frequency, such as Madden–Julian oscillation and westerly wind bust (e.g., [14]). Hence, the model that fails to capture the stochastic wind forcing tends to make a false prediction of El Niño and produce large prediction errors [15]. On the other hand, from the perspective of the model itself, one common view is that prediction uncertainties are attributed to imperfect models and initial errors. Lorenz (1975) separated two kinds of predictability problems [16]: the first is involved with the initial value problem, while the second is related to model uncertainties. Therefore, to reduce the prediction uncertainties, it is necessary to explore the cause and mechanisms that induce prediction errors from the perspective of initial condition (IC) errors and model errors [17,18], respectively.

The prediction errors caused by IC errors have been explored in-depth. For example, Xue et al. (1997) investigated the IC errors that have the fastest growth in an intermediate

coupled model developed by Zebiak and Cane (1987) (hereafter referred to as the ZC model, [7]) by using a linear singular vector (SV) approach [19]. They showed that an east–west dipole SST initial error mode in the tropical Pacific is favorable for the error growth of the SST associated with ENSO forecasts. A similar result was also reported by Tang et al. (2006) using a fully coupled global climate model [20]. Mu et al. (2003), considering the linear limitation of SV, extended the SV to a nonlinear field and proposed a condition nonlinear optimal perturbation (CNOP) approach [21]. Based on the CNOP approach, it is found that prediction errors for tropical SST caused by the CNOP-type IC errors (denoted as CNOP-I) are strongly season-dependent [22] and are highly related to the phenomenon of “spring predictability barrier” (SPB) for El Niño prediction [23]. These above studies provide a solid basis for the improvement of El Niño prediction level by improving the accuracy of ICs through target observation [24], data assimilation, and ensemble prediction [25].

The other topic for the predictability problem is related to model errors [26–28]. Given that the prediction model serves as an approximation to the Earth system, significant uncertainties exist in model parameters (MPs). Previous research has indicated that the simulation of El Niño variability can be attributed to MPs [29–31]. For instance, Zhang et al. (2013) revealed that the MPs that represent the strength of the thermocline feedback play a crucial role in the evolution of SST anomaly in the tropical Pacific [32]; Mu et al. (2010) used an updated CNOP approach (denoted by CNOP-P) to address the parametric uncertainty that influences the prediction most [18] and Duan and Zhang (2010) adopted this approach to reveal the relationship between SPB phenomenon and CNOP and showed the trivial role in causing SPB [33]. Additionally, Yu et al. (2012) suggested that MP errors have little effect on causing SPB phenomena [34], contrasting with Wu et al. (2016), who discovered that optimizing spatial distributions of parametric values can extend prediction durations and mitigate SPB occurrences in El Niño predictions [35]. Tao et al. (2019) also examined the role of space-varying MP errors and showed that the CNOP-P has the potential to cause a significant SPB for El Niño prediction [36]. The varying conclusions regarding the role of MP uncertainties in causing SPB may stem from different models utilized or the consideration of spatial variability of parametric errors in subsequent studies.

An intriguing question awaits investigation: in a practical prediction model where both initial conditions (IC) and model parametric (MP) errors can lead to SPB in El Niño forecasts, what distinguishes the roles of IC errors from those of MP errors in inducing SPB, and what mechanisms underlie their respective contributions? Addressing these queries is essential for enhancing the forecast accuracy of El Niño events. Furthermore, a comparison will be made on the sensitivity of El Niño prediction uncertainties to IC and MP errors and their dependency on the prediction timeframe, aiming to deepen comprehension of ENSO predictability dynamics and offer insights for enhancing forecasting precision of ENSO events.

The remainder of the paper is organized as follows. The methodology, including the seasonal-interannual forecast model and CNOP approach, is briefly introduced in Section 2. In Section 3, the different roles played by IC and MP errors in SPB-associated error growth are analyzed in great detail. Section 4 examines the sensitivity of the El Niño prediction to uncertainties in ICs and MPs. Section 5 investigates the impact of errors in ICs and MPs on El Niño prediction with various prediction lengths. Finally, a summary and discussion are presented in Section 6.

2. Model and Methodology

In this paper, an intermediate coupled model (ICM) developed by Zhang et al. (2003) [37] is adopted to investigate the roles of the MP and IC errors. This model has been widely used to study the variability and the predictability of El Niño [31,38–41]. Furthermore, due to the good performance in the ENSO prediction, the real-time predictions by the ICM have been contained in the routine monthly assessments of the ENSO events made by the International Research Institute of Columbia University for routine monthly

assessments (see <http://iri.columbia.edu/our-expertise/climate/forecasts/enso/current> (accessed on 26 March 2024)) and released globally. Similar to other ENSO models, the El Niño predictions made by the ICM also often suffer from the SPB phenomenon caused by the initial and parametric uncertainties [40,41]. To explore the respective roles of initial and model errors and identify many important ones in causing the SPB, the CNOP approach, as mentioned in the introduction, is used to reveal the initial or/and model parametric errors that cause the largest prediction errors.

2.1. The ICM

The ICM is a dynamic-statistical model in which a dynamical intermediate ocean model (IOM) is coupled with an empirically determined wind anomaly (denoted as τ) model. The wind anomaly model only describes the interannual variability of the wind stress but filters the wind with higher frequency since El Niño is mainly affected by the interannual variability of the wind. The IOM describing the evolution of the surface current in the tropical Pacific is a nonlinear model that only produces the time-evolution of the zonal and vertical current anomalies over the mixed layer of the tropical Pacific and the sea level (SL) anomaly. Additionally, to represent the thermodynamics that are forced by the ocean current anomalies, an SST anomaly model is embedded into the IOM to yield the evolution of the SST anomaly. The SST anomaly model can be written as follows:

$$\begin{aligned} \frac{\partial T'}{\partial t} = & -u' \frac{\partial \bar{T}}{\partial x} - (\bar{u} + u') \frac{\partial T'}{\partial x} - v' \frac{\partial \bar{T}}{\partial y} - (\bar{v} + v') \frac{\partial T'}{\partial y} \\ & - \{ (\bar{w} + w') M(-\bar{w} - w') - \bar{w} M(-\bar{w}) \} \frac{(\bar{T}_e - \bar{T})}{H} \\ & + \frac{\kappa_h}{H} \nabla_h \cdot (H \nabla_h T') + \frac{2\kappa_v}{H(H+H_2)} (T'_e - T') \\ & - (\bar{w} + w') M(-\bar{w} - w') \frac{(T'_e - T')}{H} - \alpha_T T' \end{aligned} \tag{1}$$

Note that the thermocline fluctuations or subsurface processes play dominant roles in SST diversity and variability [7,42]. As such, Zhang et al. (2003) developed a T_e model into the SST model to represent the thermocline effect on the SST [37]. Due to the SL anomaly can characterize the perturbation of thermocline (or subsurface temperature) to some extent, there exists a strong relationship between the SL and T_e anomaly. Given this, the T_e model is built based on the relationship between the SL anomaly and subsurface entrainment temperature (T_e), which is defined as follows:

$$T_e = \alpha_{T_e} \cdot F_{T_e}(X_{SL}) \tag{2}$$

in which F_{T_e} denotes the statistical relationship between SL and T_e anomaly. Here, an added α_{T_e} parameter is used to represent the intensity of SST-thermocline feedback.

A similar scheme is applied to the τ model. The τ model is constructed based on the highly coupling SST and wind fields, which can be expressed as follows:

$$\tau = \alpha_\tau \cdot F_\tau(X_{SST}), \tag{3}$$

where F_τ is the relationship between SST anomaly and τ according to the historical data, and α_τ represents the intensity of the SST-wind feedback. Previous studies indicated that the SST evolution simulated by the ICM is related to the values of α_{T_e} and α_τ [31,32]. In the present study, the $\alpha_{T_e} = 1.0$ and $\alpha_\tau = 0.87$ are predetermined so that the ICM can well represent the interannual variability of SST. For further details on the ICM, see [38].

2.2. The CNOP Approach and Experimental Design

2.2.1. Mathematical Expression of the CNOP

The CNOP approach is proposed by Mu et al. (2003) to search for the optimal perturbation that can lead to the largest error growth in a nonlinear system. Due to the advantage of dealing with nonlinear problems, the CNOP has been widely used to study the pre-

dictability of chaotic systems [22]. The main idea of the CNOP approach is described in this section. More details are referred to [18].

Supposing a nonlinear model that represents the climate system is denoted as \mathcal{M} , given the model parameter \mathbf{p} and initial states \mathbf{X}_0 , the model results at time T can be defined as $\mathbf{Y} = \mathcal{M}(\mathbf{X}_0, \mathbf{p})(T)$. Here, we can call \mathbf{Y} the reference state. When perturbing the MPs and ICs (e.g., \mathbf{u}_0 for ICs and \mathbf{p}' for MPs), a new solution is obtained as $\mathbf{Y} + \mathbf{Y}' = \mathcal{M}(\mathbf{X}_0 + \mathbf{u}_0, \mathbf{p} + \mathbf{p}')(T)$. Obviously, \mathbf{Y}' is the error growth induced by the combined effect of MPs and ICs. The CNOP approach aims to solve the following optimization problem within a certain constraint $(\mathbf{u}_0, \mathbf{p}') \in C$:

$$J(\mathbf{u}_0^*, \mathbf{p}^*) = \max_{(\mathbf{u}_0, \mathbf{p}') \in C} J(\mathbf{u}_0, \mathbf{p}') = \max_{(\mathbf{u}_0, \mathbf{p}') \in C} \|\mathcal{M}(\mathbf{X}_0 + \mathbf{u}_0, \mathbf{p} + \mathbf{p}')(T) - \mathcal{M}(\mathbf{X}_0, \mathbf{p})(T)\|^2, \quad (4)$$

in which $\|\cdot\|$ is the L2-norm used to measure the error growth \mathbf{Y}' and J is the object function. The optimized perturbations $(\mathbf{u}_0^*$ and $\mathbf{p}^*)$ are the so-called CNOPs. From Equation (4), the CNOP approach has the ability to search optimal perturbations that cause the largest error growth. The obtained J quantifies the maximum impact of the perturbation on the prediction of the reference state \mathbf{Y} . As the obtained J is larger, the model is more sensitive to the corresponding perturbation. Much more detail about the CNOP approach is referred to [18,21].

Then, if we only consider the uncertainties in the ICs and the model is assumed to be perfect, the optimization problem is modified as follows:

$$J(\mathbf{u}_0^*) = \max_{\mathbf{u}_0 \in C_I} J(\mathbf{u}_0) = \max_{\mathbf{u}_0 \in C_I} \|\mathcal{M}(\mathbf{X}_0 + \mathbf{u}_0, \mathbf{p})(T) - \mathcal{M}(\mathbf{X}_0, \mathbf{p})(T)\|^2, \quad (5)$$

where \mathbf{u}_0^* is the most unstable IC errors (referred to as CNOP-I) that can make the prediction deviate from the reference state most (see [40]).

If we only consider the errors in MPs rather than ICs, the CNOP approach is used to solve the problem as follows:

$$J(\mathbf{p}^*) = \max_{\mathbf{p}' \in C_P} J(\mathbf{p}') = \max_{\mathbf{p}' \in C_P} \|\mathcal{M}(\mathbf{X}_0, \mathbf{p} + \mathbf{p}')(T) - \mathcal{M}(\mathbf{X}_0, \mathbf{p})(T)\|^2. \quad (6)$$

The optimized \mathbf{p}^* is the optimally growing MP errors (denoted by CNOP-P) when the ICs are perfect (Tao et al. 2019 [36]).

2.2.2. Designs of the CNOP Experiments

Since the Bjerknes positive feedback is the main mechanism dominating the development of El Niño [43], the uncertainties of El Niño prediction are commonly related to the uncertainties of the Bjerknes feedback. The Bjerknes feedback consists of three sub-processes: the SST-wind feedback, the wind-SL feedback, and the thermocline-SST feedback. On the one hand, it is clear that the SST and thermocline are the key oceanic variables in the Bjerknes feedback, which are respectively related to the SST-wind and thermocline-SST feedback. On the other hand, the strengths of SST-wind and thermocline-SST feedback are explicitly denoted as α_τ and α_{T_e} in the ICM, respectively. Therefore, two ICs, i.e., SST and SL, and these two MPs are perturbed in CNOP analyses to explore the El Niño predictability.

To perform the CNOP approach, the constraint functions for IC errors are defined as follows:

$$\delta_{\text{SST}} = \sqrt{\frac{1}{N} \sum_{i,j} [\text{SST}'(i,j)]^2}, \delta_{\text{SL}} = \sqrt{\frac{1}{N} \sum_{i,j} [\text{SL}'(i,j)]^2}, \quad (7)$$

where $SST'(i, j)$ and $SL'(i, j)$ are the perturbations of SST and SL in the grid (i, j) , respectively, and N is the total number of the model grid over the tropical Pacific, excluding the model land. Similarly, the constraint functions for MPs are described as follows:

$$\delta_{\tau} = \sqrt{\frac{1}{N} \sum_{i,j} [p'_{\tau}(i, j)]^2}, \delta_{T_e} = \sqrt{\frac{1}{N} \sum_{i,j} [p'_{T_e}(i, j)]^2}, \tag{8}$$

where p'_{τ} and p'_{T_e} are the perturbations of α_{τ} and α_{T_e} , respectively. Since the prediction of El Niño is usually involved with the SST anomaly in the tropic Pacific, the object function that quantifies prediction errors is expressed as follows:

$$J = \sqrt{\frac{1}{N} \sum_{i,j \in \Omega} [E_{SST}(i, j, T)]^2}, \tag{9}$$

where E_{SST} denotes the difference between the predicted SST anomaly at prediction time T and the reference El Niño state.

In the present study, one typical El Niño event simulated by the ICM is chosen as a reference state for investigating the sensitivity to MPs and ICs. For convenience, the year when the tropical Pacific achieves the mature phase of El Niño is denoted as year (0). The year before and after is referred to as year (−1) and year (1), accordingly. To assess the roles of the MPs and ICs in different phases (i.e., onset phase, mature phase, decay phase) predictions of the El Niño event, we make 12-month predictions at the start time of July (−1), January (0) and July (0), and correspondingly predict the SST anomalies in June (0), December (0) and June (1), respectively. The IC-related constraint radiuses δ (Equation (7)) are preliminarily determined to be 0.2 °C for SST and 1 cm for SL, which are dynamically harmonious and also approximate to the observation errors. The MP-related constraint bound δ is defined as $\delta_{\tau} \leq 2\% \cdot \alpha_{\tau}$ and $\delta_{T_e} \leq 2\% \cdot \alpha_{T_e}$, within which the ICM still has the capacity to capture the realistic interannual variability of the SST in the tropical Pacific. The former defined constraint value is the standard (reference) constraint, which will be used to compare with other CNOP experiments (Sections 4 and 5).

To compare the error growth induced by ICs and MPs, two sets of CNOP experiments are repeated as in [36,40] but with different constraints of the IC and MP errors. For the CNOP-I experiments, the ICs, including SST and SL, are perturbed under the given constraint without perturbing MPs. On the contrary, for the CNOP-P experiments, the optimal errors of MPs (α_{τ} and α_{T_e}) are calculated without adding IC errors. Since uncertainties exist in both MPs and ICs in practice, a simple comparison between CNOP-I and CNOP-P will cause the error interaction between MPs and ICs to be lost. Therefore, the CNOPs in which MPs and ICs are conditionally perturbed simultaneously are additionally performed. Physically, CNOP-I (CNOP-P) represents the optimal mode of errors in ICs (MPs) that has great potential to destroy the prediction, and CNOPs are the optimally combined mode of errors in MPs and ICs. By analyzing the CNOP information, we can determine not only the sensitive areas for prediction but also the relationship between IC/MP errors and prediction errors [36,40].

3. The Impact on Season-Dependent Error Growth

In this section, we investigate time-dependent error evolutions induced by the optimal IC errors (i.e., CNOP-I), optimal MP errors (i.e., CNOP-P), and optimally combined errors (CNOPs). The corresponding error evolutions for CNOPs, CNOP-I, and -P are nearly identical, with the largest error growth occurring in spring and yielding an SPB phenomenon. However, the hidden error growth mechanisms could be different.

3.1. Horizontal Distributions of CNOPs-Type Errors

As mentioned above, CNOP-type errors are the dominant unstable mode that induces large error growth. It is valuable to explore the spatial structure of the CNOP-type er-

rors [24]. Using the ICM, Tao et al. (2017) demonstrated CNOP-Is in different seasons [40]. Later, they investigated the horizontal distributions of CNOP-P [36] and indicated that both the CNOP-I and CNOP-P are independent of constraint value, thereby suggesting that the CNOP-determined sensitive areas are robust. However, the above studies ignored the interaction between MPs and ICs, so we still have no idea whether the optimal mode for ICs and MPs is the same or not when both errors in ICs and MPs are considered in the CNOP analysis. To answer this, we calculated the optimally combined mode of ICs and MPs (i.e., CNOPs).

Figure 1 displays the horizontal distributions of CNOPs, including ICs (SST and SL) and MPs (α_τ and α_{T_e}) for different phase predictions. It is evident that CNOPs are concentrated in a certain local region, indicating that errors in those areas are responsible for the prediction errors. Take the CNOPs in the mature phase prediction of El Niño for example; the SST and α_τ components with positive value are mainly located in the central tropical Pacific (Figure 1(b1,b3)), and the SL and α_{T_e} with positive value are concentrated in the eastern equatorial Pacific (Figure 1(b2,b4)). The structures of CNOPs are slightly changed due to different initial months, but the locations where CNOPs peak are the same: the SST and α_τ components are mainly centered in the central tropical Pacific; SL and α_{T_e} components are mainly located in the eastern tropical Pacific.

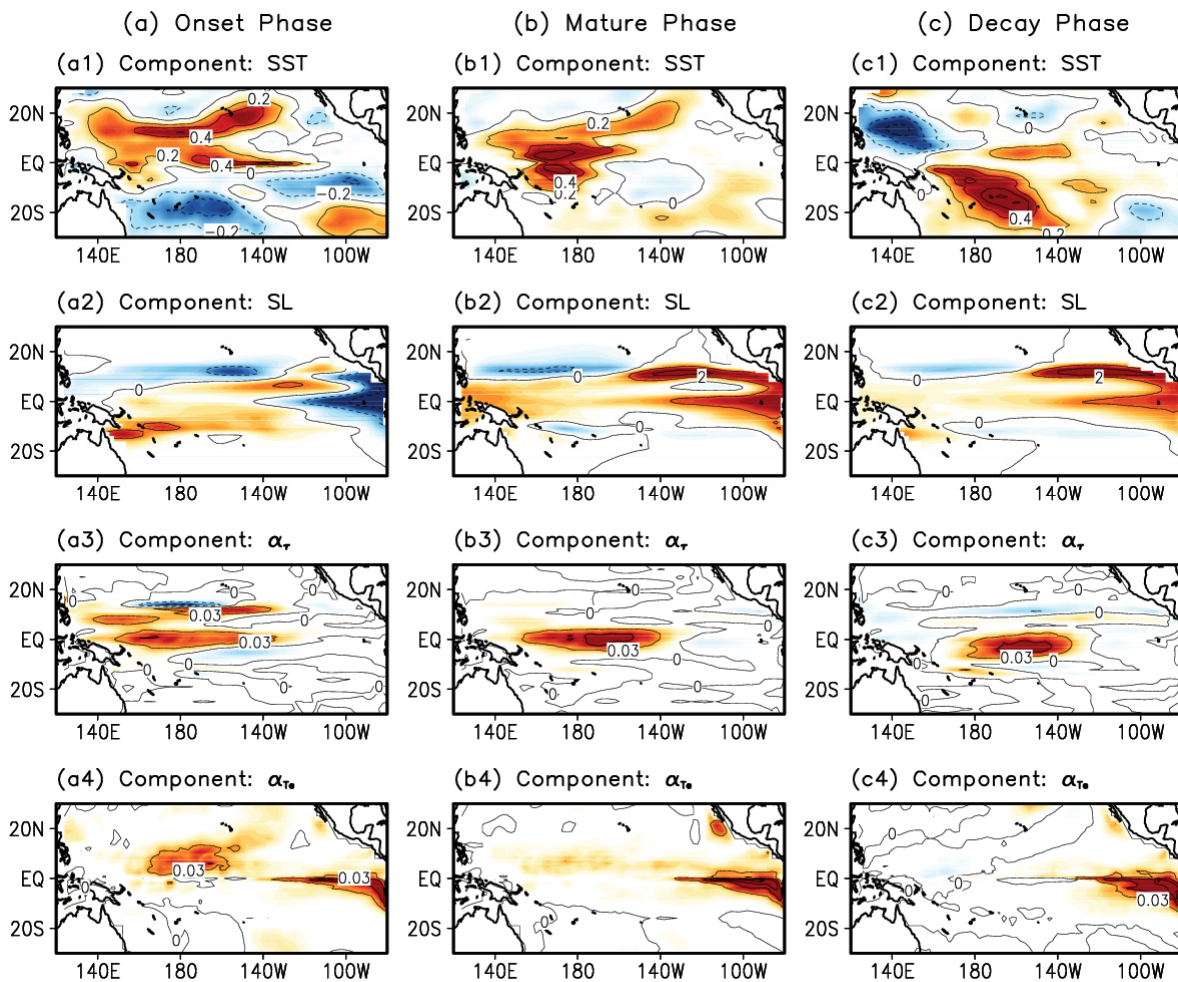


Figure 1. Horizontal distributions of the CNOPs in the (a) onset, (b) mature, and (c) decay phase predictions of El Niño. Panels from top to bottom in each column are the CNOPs component of SST, SL, α_τ and α_{T_e} , respectively. The contour interval is 0.2 °C for SST, 2 cm for SL, 0.03 for α_τ and α_{T_e} .

It is not surprising that the horizontal distributions of SST and α_τ components in CNOPs are similar, while those of SL and α_{T_e} are nearly equal. On the one hand, since the sea surface where the air–sea coupling is active is the junction of ocean and atmosphere, the SST as the production of air–sea coupling and α_τ representing the strength of air–sea coupling are interrelated dynamically. On the other hand, the SL represents the subsurface signal to some extent, which affects the surface through thermocline feedback. Thus, the SL and α_{T_e} are also interrelated in dynamic.

Another interesting finding is that CNOPs are roughly the linear combination of CNOP-I and CNOP-P. The MPs components of CNOPs are similar to the CNOP-P in both horizontal pattern and phase (not shown, referred to [36]). The IC components of CNOPs are the same as the CNOP-I (not shown, referred to [40]) but with opposite phases. That is, CNOPs = –CNOP-I + CNOP-P. The comparison indicates that the interaction between MPs and ICs does not change the horizontal characteristics of CNOPs but phases. Additionally, it seems that MP errors are more important than IC errors in El Niño prediction since the optimal mode of MPs is constant while the optimal mode of ICs is phase-inversed when considering the interaction of the ICs and MPs.

3.2. Error Evolution

To examine to what extent errors in ICs and MPs affect predictions, we further analyze the prediction errors and evolutions. By comparing the reference state with predictions perturbed by CNOP, we identified the prediction errors attributed to CNOP-type errors for each variable. It is observed that the final predicted SST errors induced by CNOP-P are different from those induced by CNOP-I. For the CNOP-P case, a positive SST error was detected in the eastern Pacific cold tongue region due to the intensified Bjerknes feedback caused by CNOP-P, leading to an overestimation of El Niño strength [36]. As a result, the model tends to predict a stronger-than-reference El Niño. On the contrary, in the CNOP-I case, a weaker-than-reference El Niño is predicted as negative initial errors are amplified through air–sea coupling. It seems that the MP errors likely counteract the effect of IC errors in predictions if the CNOP-I and CNOP-P are directly added to the ICM. However, that is not the case. As mentioned in Section 3.1, not only has the optimal error mode for SST changed, but the error growth has also increased due to the interaction of ICs and MPs. The CNOPs with positive errors in ICs and MPs tend to predict a stronger El Niño. In other words, the prediction error induced by the CNOPs is as positive as that by CNOP-P, but the former is larger.

To figure out how prediction errors come about for the CNOPs case, we next study the underlying mechanisms from the perspective of error growth.

The error evolutions for SST, wind stress, and SL that are induced by CNOPs in different phase predictions are displayed in Figure 2. Generally, CNOPs tended to produce an El Niño-like SST error pattern in 12-month predictions. However, the temporal evolution of prediction errors varied across different phases. When predicting the onset phase of El Niño, the initial SL error is negative around the cold tongue region (Figure 1(a2)), and the model has strong SST-thermocline feedback in the eastern Pacific (Figure 1(a4)). As a result, the cold signal in the subsurface continually penetrates the surface through thermocline fluctuations, leading to (+, –) dipole distribution for SST error (i.e., positive signal in the central Pacific and negative signal in the eastern tropical Pacific). Such SST error distribution enhances the trade wind that, in turn, exacerbates upwelling in the cold tongue, so the model tends to predict a colder ocean at the 6-month leading time. In Dec (0), remarkable errors were found in the zonal wind over the western Pacific, causing a stronger-than-normal recharge (revealed by significant positive SL errors in the western Pacific). The over-predicted westerly wind triggers excessive downwelling that propagates eastward by Kelvin waves. Subsequently, the prediction errors with negative values in the central Pacific are reduced and turn positive. The westerly wind is further enlarged for enhanced SST-wind feedback (indicated by the positive errors in α_τ in the central tropical Pacific). The dynamic effect of the westerly wind is to deepen the thermocline and warm

up the central-eastern equatorial Pacific. Therefore, the CNOPs cause El Niño-like errors when predicting the onset phase of El Niño. Differing from the onset phase prediction that SST error experiences phase change, positive SST errors prevail throughout the prediction period for the case of the mature phase prediction. This is not only due to the initial Bjerknes feedback built up by the warmer initial SST and SL (Figure 1(b1,b2)) but also due to the enhanced Bjerknes feedback reflected by the enlarged α_τ and α_{Te} (Figure 1(b3,b4)). Therefore, the prediction errors in the mature phase prediction are larger than in the onset phase prediction. For the case of the decay phase prediction, the prediction error for SST in the eastern tropical Pacific is positive, while the SST error in the central tropical Pacific evolved from a positive to a negative value. This is because the negative initial SST error in the western Pacific (Figure 1(c1)) is propagated easterly under an enhanced Bjerknes feedback system. Broadly, although the error evolutions are not the same for different phase predictions, the over-predicted El Niño is attributed to the enhanced Bjerknes feedback that amplifies the IC errors, which are propagated eastward by ocean waves over time.

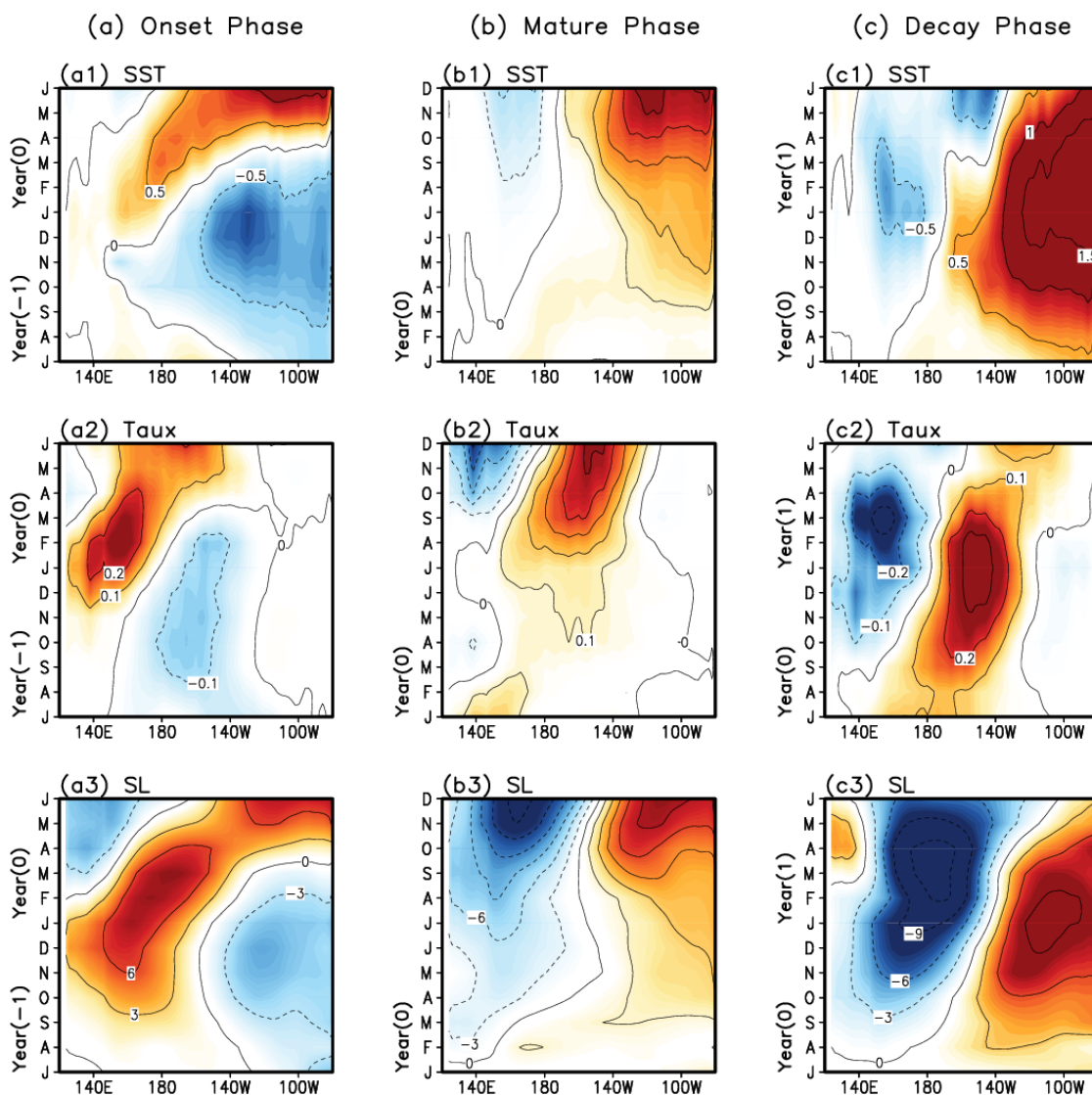


Figure 2. Longitude–time sections of the CNOPs-induced prediction errors along the equator during the (a) onset, (b) mature, and (c) decay phase predictions. Panels from top to bottom in each column are the prediction errors in SST, zonal wind stress, and SL, respectively. The contour interval is 0.5 °C for SST, 0.1 dyn cm⁻² for wind stress, and 3 cm for SL. The CNOP-I and CNOP-P-induced error evolutions are referred to by Tao et al. (2017) [40] and Tao et al. (2019) [36], respectively.

To compare error evolutions caused by CNOP-I, CNOP-P, and CNOPs, we calculate the correlation coefficient between CNOPs and CNOP-I (CNOP-P) for each variable error within a 12-month prediction. The results for onset and decay phase predictions are shown in Figures 3 and 4, respectively. It is found that the SST error evolutions caused by the CNOPs are nearly identical to that caused by the CNOP-P (the correlation is close to 1) but contrary to that by the CNOP-I (the correlation is close to -1). This suggests that the CNOP-P and CNOPs share the same error evolution, giving rise to an El Niño-like SST error, and the CNOP-I holds the opposite role and causes a La Niña-like error evolution. It should be pointed out that the behavior of CNOPs that tends to generate positive rather than negative error growth also reflects the nature of ENSO asymmetry (i.e., the amplitude of the warm phase is generally larger than the cold phase). The CNOP-P has the potential to inherit CNOPs, while the CNOP-I does not always induce error growth that is consistently parallel to the CNOPs case. For example, as shown in Figure 4a, the correlation between CNOPs and CNOP-I cases has a noticeable variation along the equator, ranging from -0.9 to 0.9 . In particular, the error evolution caused by the CNOP-I in the western Pacific is unrelated to that by CNOPs (the correlation is nearly 0).

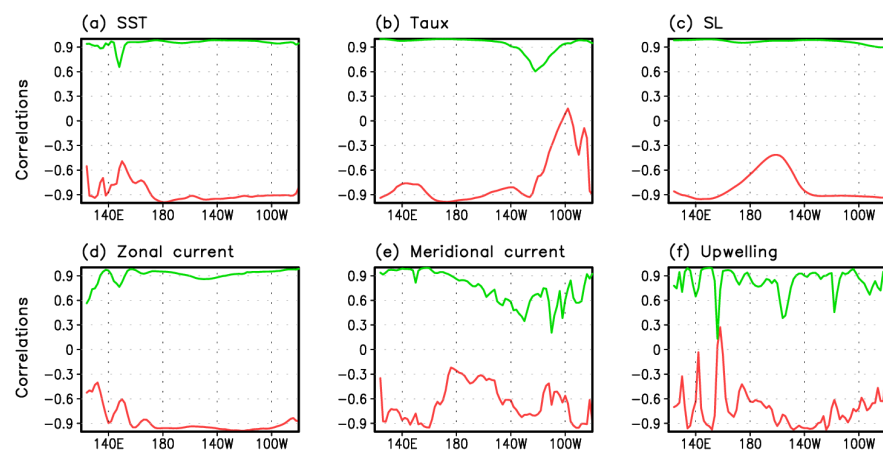


Figure 3. Correlation coefficients of the prediction errors in (a) SST, (b) zonal wind stress, (c) SL, (d) zonal current, (e) meridional current, and (f) vertical current, over 12-month prediction for the onset phase of El Niño. The correlation between CNOP-I (CNOP-P) and CNOPs-induced errors are denoted as red (green) curves. Note that only SST errors consistently show a high correlation while other variables do not, implying that the underlying mechanisms accounting for the SST error evolution are different by the CNOP-I and CNOP-P.

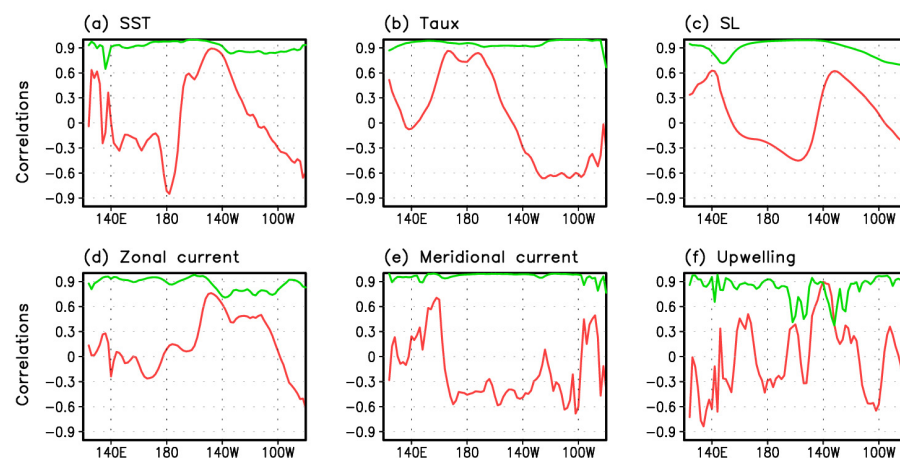


Figure 4. The same as Figure 3 but for the decay phase prediction.

3.3. Mechanism for SPB-Associated Error Evolution

Previous studies have unequivocally demonstrated that both CNOP-I and CNOP-P can trigger SPB-associated error evolutions [36,40]. In this section, we not merely illustrate the temporal SST error evolutions triggered by CNOP-I, CNOP-P, and CNOPs but also delve deeper into distinguishing their dynamic disparities.

Figure 5 shows the SST errors in the Niño3.4 area and the corresponding tendencies for different phase predictions. We focus on the SST errors in the Niño3.4 area because it is the main benchmark for judging the prediction of the El Niño event internationally. Consistent with Figure 3, CNOP-I tends to generate a negative error, while CNOPs and CNOP-P are likely to cause positive errors. One may note that all CNOP-type errors tend to cause negative SST errors in the Niño3.4 area when predicting the decay of El Niño (Figure 5c). In fact, the CNOP-P and CNOPs-induced SST error features a dipole mode (the positive error in the eastern tropical Pacific and the negative error in the central Pacific) when predicting the decay phase of El Niño (Figure 2c). Despite these patterns, a substantial error growth tendency is observed in late winter and spring (i.e., from January to April) across all predictions. Taking the onset phase prediction as an example, the strongest negative tendency induced by CNOP-I peaks in February, further amplifying the negative error at the end of the prediction. The largest error tendency caused by CNOP-P (exceeding 0.1 °C/month) occurs around April. The strong effect induced by the CNOP-P in the spring pulls the SST prediction from a negative error to a positive error at the end of the prediction. When the effect of ICs and the MPs are considered simultaneously, the error growth tendency becomes larger with the peak tendencies of 0.4 °C/month between March and April.

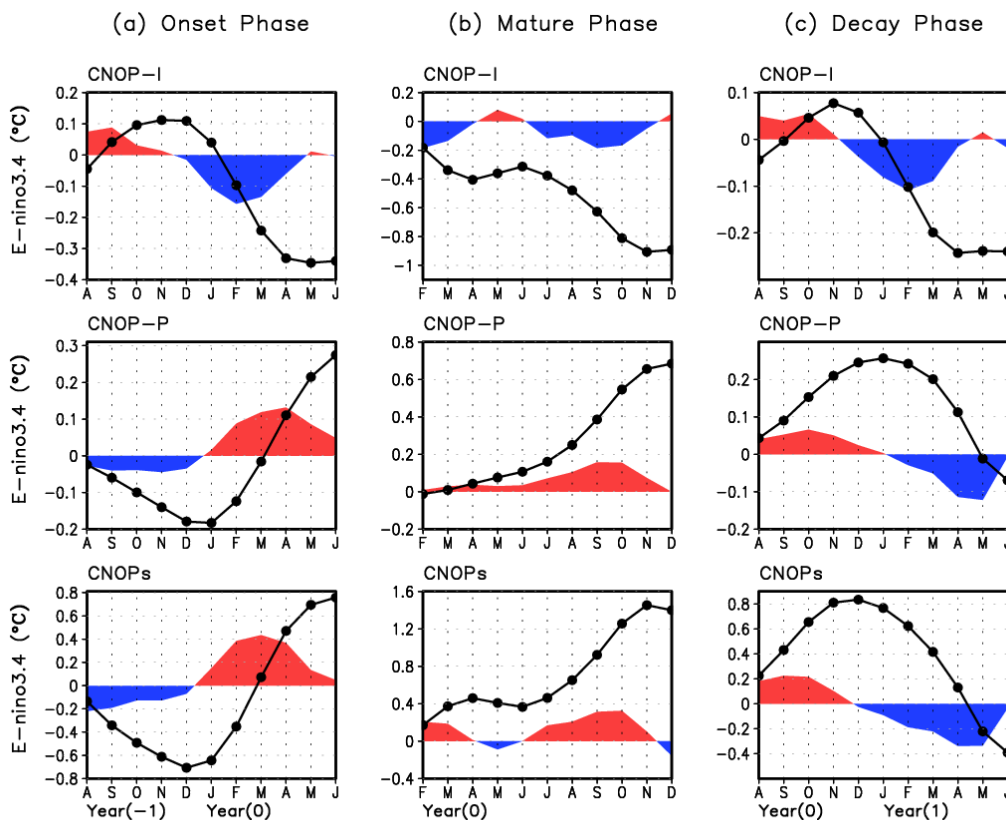


Figure 5. The prediction SST errors (unit: °C) in the Niño3.4 area (denoted as E-Niño3.4; black line) and corresponding tendency errors (shaded area; unit: °C/month) in the (a) onset, (b) mature, and (c) decay phase predictions of El Niño. From top to bottom are cases for the CNOP-I, CNOP-P, and CNOPs, respectively.

Although the SST error evolution, including the SPB-associated error growth, exhibits a strong similarity in the Niño3.4 area (with correlations close to -1 or 1 , as shown in Figures 3a and 4a), this similarity does not extend to other variables. As shown in Figure 3, the correlation between error evolutions in meridional and vertical currents is nearly nonexistent in certain regions when comparing the CNOP-I and CNOPs cases. Especially for the decay phase prediction (Figure 4), CNOP-I-induced error evolution is totally different from CNOP-P or CNOPs. It is implied that the IC-induced and MP-induced SPB have different mechanisms.

To explore and distinguish the mechanisms for the large error growth in spring, we calculate each term (i.e., heat budget term) of the tendency error, including vertical convection, zonal, and meridional advectons in the mixed layer from February to April. Figure 6 displays the distributions of the heat budget in the spring. It is of interest that the error of the vertical convection of the mean temperature by the anomalous upwelling, namely the Ekman pumping feedback (i.e., $w' \frac{\partial \bar{T}}{\partial z}$, denoted as VC_{am}), is so small that it hardly contributes to the error growth whether caused by errors in ICs or MPs, suggesting that the prediction of vertical current is not sensitive to the ICs or MPs in spring. However, as implicated in Figures 3 and 4, the dominant terms causing the SPB are dependent on the error sources (i.e., errors in the ICs or MPs) and phase predictions.

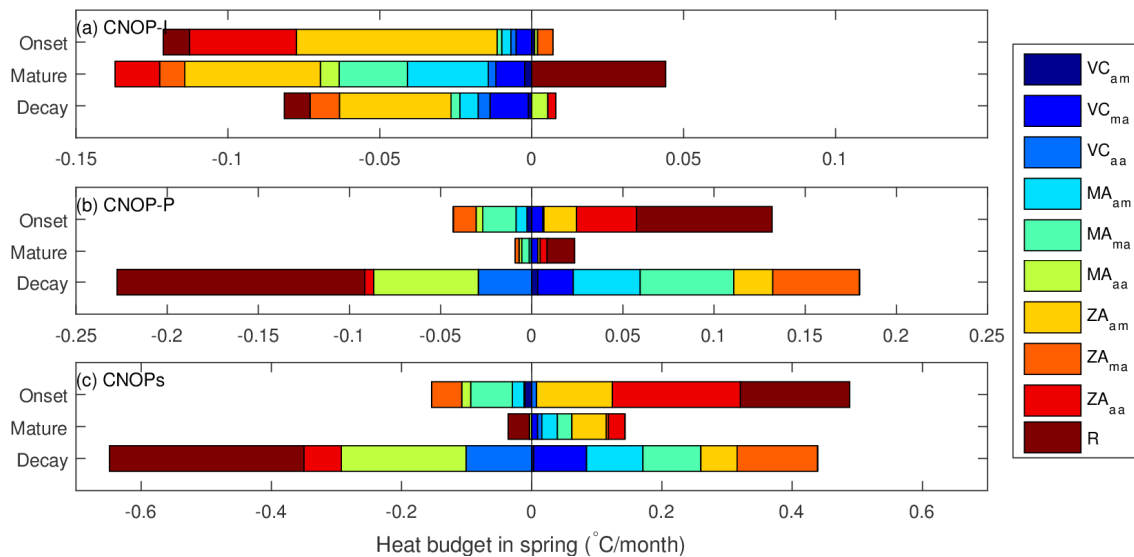


Figure 6. Distributions of tendency errors in each term (unit: $^{\circ}\text{C}/\text{month}$) in the spring that are caused by the (a) CNOP-I, (b) CNOP-P, and (c) CNOPs. Results for different phase predictions of El Niño are shown along the y-axis in each panel. The colored bars (see graph legend in the right panel) represent error tendency terms from the heat budget analysis. For convenience, the vertical convection (VC) of the anomalous upwelling and mean temperature ($w' \frac{\partial \bar{T}}{\partial z}$) is denoted as VC_{am} , and that of the anomalous upwelling and anomalous temperature ($w' \frac{\partial T'}{\partial z}$) is denoted as VC_{aa} , and so are the zonal advection (ZA) and meridional advection (MA). The residual term, including the heat flux, diffusion, and conduction, is denoted as R.

The distribution of each error tendency term that is caused by the CNOP-I for different phase predictions is shown in Figure 6a. It was found that error in the zonal advection is the dominant term, contributing more than 60% to the total tendency error in spring, followed by the meridional advection. Particularly, uncertainties in the zonal advection term are mainly dependent on the mean temperature and the anomalous zonal current [i.e., zonal advection feedback ($u' \frac{\partial \bar{T}}{\partial x}$), denoted as ZA_{am}]. The vertical advection (the blue bars) also enhances the SPB in CNOP-I cases. The above results manifest that errors in ICs tend to perturb the ocean current, giving rise to large uncertainties in advection terms, which accounts for the large error growth in spring for the El Niño prediction. In this light,

improving the prediction of ocean currents is a priority to improve the El Niño prediction using the ICM when the ICs are not perfect.

However, the advection terms are more likely to have a negative effect on the error growth in spring when errors exist in MPs. The heat budget for the CNOP-P case is shown in Figure 6b. Clearly, it is different from the CNOP-I case (Figure 6a). We observe that the remainder term (i.e., the heat flux, diffusion, and conduction terms, and the brown bar in Figure 6) is the chief culprit destroying prediction in the spring. Positive values of these remainder terms contribute to positive SST errors, particularly when predicting the onset and mature phases of El Niño, as shown in Figure 5a,b. Conversely, during the decay phase prediction, negative values of the remainder term led to negative SST errors in the model employing CNOP-P, as illustrated in Figure 5c. Interestingly, advection terms generally play a minimal role in SPB-related evolution and may even hinder error growth in spring, with the exception of nonlinear terms. For example, the growth rate explained by the residual term is up to $-0.15\text{ }^{\circ}\text{C}/\text{month}$ in spring during the decay phase prediction, while the total error growth rate is only $-0.05\text{ }^{\circ}\text{C}/\text{month}$ because of the negative effect of the MA_{am} and MA_{ma} (about $0.05\text{ }^{\circ}\text{C}/\text{month}$ and $0.03\text{ }^{\circ}\text{C}/\text{month}$, respectively). From the above, it becomes evident that the SPB phenomenon triggered by MP errors is primarily attributable to uncertainties in thermodynamic processes. Therefore, we suggest that we should take care of the simulations of the thermodynamics (i.e., the heat flux, diffusion, and conduction terms) in El Niño prediction when MPs or the strength of the Bjerknes feedback are not realistic in the ICM.

The case is much more complicated when errors exist in both ICs and MPs. Figure 6c displays errors in each term of the tendency that are induced by the CNOPs. Although the evolution of sea surface temperature (SST) errors induced by the CNOP-P closely resembles that caused by CNOPs, the processes underlying the SPB differ somewhat. Influenced by the IC errors, the residual term fails to adequately account for the large error growth in spring. In particular, when predicting the maturity of the El Niño, almost all tendency terms exhibit a positive impact on error growth, with the exception of the residual term. Additionally, the effects of nonlinear terms become larger and even exceed the residual term.

Another intriguing finding is the emergence of significant error growth not only in spring but also in fall during the prediction of the mature phase (Figure 5b). As mentioned above, the SPB-associated error growth mechanisms induced by the ICs and MPs are entirely different, although they are all forced by the Bjerknes feedback: the former is primarily due to the advection processes, while the latter is attributed to the thermodynamics. Then, what about the fall error growth? To compare the differences caused by the ICs and MPs, we also present the uncertainties in the heat budget in the fall (shown in Figure 7). Different from the strong error growth in spring, processes evoked by IC errors are surprisingly similar to that by MP errors in fall, that the fall error growth is mainly caused by the uncertainties in linear advection terms (e.g., $u'\frac{\partial T'}{\partial x}$, $\bar{u}\frac{\partial T'}{\partial x}$, $\bar{w}\frac{\partial T'}{\partial z}$). The residual term and nonlinear advectons tend to show a negative effect against the large error growth. Not only that, the combined error mode of ICs and MPs (i.e., CNOPs) also has the same error growth mechanisms, suggesting that the mechanism of the fall error growth is unrelated to the errors in the ICs or MPs.

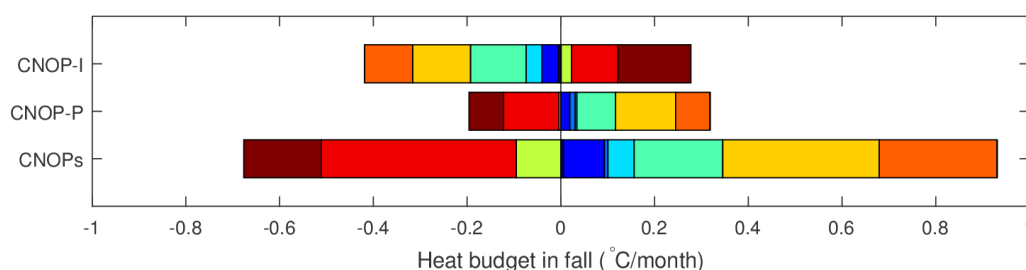


Figure 7. The same as Figure 6 but for the error growth in fall.

4. The Sensitivity of Predictions to Uncertainties in ICs and MPs

Since the roles of ICs and MPs in SPB-associated error evolutions are found to be different in the last section, it is conceivable that the sensitivities of El Niño prediction to uncertainties in ICs and MPs are also not the same.

Three sets of sensitivity experiments are designed to examine uncertainties of El Niño prediction arising from errors in ICs and MPs. The first set of experiments (referred to as IC perturbed experiments, including SST perturbed and SL perturbed experiments) shown in Table 1 is performed to compare the sensitivity of El Niño prediction to the magnitudes of uncertainties in the SST and SL, in which only the constraints of SST and SL are changed but without MPs errors in CNOP analysis. Take the case of SST perturbed experiments; for example, constraint 2 means that the constraint bound δ for initial SST is $2 \times 0.2 \text{ }^\circ\text{C}$, and 3 means $3 \times 0.2 \text{ }^\circ\text{C}$. The IC perturbed experiments can reveal the relative importance between initial SST and SL during El Niño prediction. In addition to the SST and SL signal, the corresponding processes (i.e., α_τ and α_{Te}) are also important in El Niño development. Although Gao and Zhang (2017) [31] have investigated the contributions of SST-wind and SST-thermocline feedback to the evolution of SST anomaly in the tropical Pacific, the issue of which process is dominant is yet unclear. Therefore, the second set of sensitivity experiments (referred to as MP perturbed experiments) shown in Table 2 is designed to explore the relative contribution of α_τ and α_{Te} . The third set of sensitivity experiments (denoted as IC-MP experiments) shown in Table 3 will reveal the relative importance of errors in ICs and MPs in El Niño prediction. The IC-MP-1 (IC-MP-2) experiments are related to the CNOP-I (CNOP-P) experiments in which MP (IC) errors are ignored. In the IC-MP-3 experiment, the constraints of ICs and MPs are changed simultaneously from 0 to 4, which is in comparison with the IC-MP-1 (IC-MP-2) experiments. The combined effect (CE) is calculated using the equation $CE = \frac{J_{IP} - (J_I + J_P)}{J_I + J_P}$, in which J_I and J_P are the final error induced by the CNOP-I and CNOP-P, respectively; J_{IP} is the prediction error induced by the CNOPs.

Table 1. Settings of the IC perturbed experiments based on the CNOP-I approach, in which the MP errors are ignored. To examine the sensitivity of El Niño prediction to uncertainties in the SST of the ICs, the initial SST constraint intensity that represents the relative constraint to the standard case in Section 2.2.2 is changed from 0 to 4 with the initial SL constraint fixed. Analogously, to explore the sensitivity to uncertainties in the initial SL, the initial constraints are unfixed for the SL but fixed for the SST.

Experiments		IC Constraint	
		SST	SL
IC perturbed experiments	SST	$\delta_{SST} = (0, 0.5, 1, 2, 3, 4) \cdot \delta_{SST}^*$	$\delta_{SL}^* = 1 \text{ cm}$
	SL	$\delta_{SST}^* = 0.2 \text{ }^\circ\text{C}$	$\delta_{SL} = (0, 0.5, 1, 2, 3, 4) \cdot \delta_{SL}^*$

Table 2. Settings of the MP perturbed experiments based on the CNOP-P approach, in which the IC errors are ignored. Similar to the IC perturbed experiments in Table 1, two types of experiments are designed to explore the prediction sensitivity to uncertainties in two MPs, one of which has unfixed constraints ranging from 0 to 4, and the other one is fixed. The reference MPs are $\alpha_{Te} = 1.0$ and $\alpha_\tau = 0.87$.

Experiments		MP Constraint	
		α_τ	α_{Te}
MP perturbed experiments	α_τ	$\delta_\tau = (0, 0.5, 1, 2, 3, 4) \cdot \delta_\tau^*$	$\delta_{Te}^* = 2\% \cdot \alpha_{Te}$
	α_{Te}	$\delta_\tau^* = 2\% \cdot \alpha_\tau$	$\delta_{Te} = (0, 0.5, 1, 2, 3, 4) \cdot \delta_{Te}^*$

Table 3. Settings of the IC-MP experiments that were used to explore the combined effect of the ICs and MPs. The IC-MP-1 experiment is related to the standard CNOP-I analysis, in which the constraints of two ICs are changed simultaneously from 0 to 4, but the MP errors are ignored. The IC-MP-2 experiment is related to the standard CNOP-P analysis in that the IC errors are ignored. The third type of experiment is designed to explore the combined effect of ICs and MPs, in which the constraints of the ICs and MPs are changed in a synchronous manner in the CNOPs analysis.

Experiments	IC Constraint	MP Constraint	
IC-MP experiments	IC-MP-1	$(\delta_{SST}, \delta_{SL}) = (0, 0.5, 1, 2, 3, 4) \cdot (\delta_{SST}^*, \delta_{SL}^*)$	$(\delta_{\tau}, \delta_{Te}) = 0$
	IC-MP-2	$(\delta_{SST}, \delta_{SL}) = 0$	$(\delta_{\tau}, \delta_{Te}) = (0, 0.5, 1, 2, 3, 4) \cdot (\delta_{\tau}^*, \delta_{Te}^*)$
	IC-MP-3	$(\delta_{SST}, \delta_{SL}, \delta_{\tau}, \delta_{Te}) = (0, 0.5, 1, 2, 3, 4) \cdot (\delta_{SST}^*, \delta_{SL}^*, \delta_{\tau}^*, \delta_{Te}^*)$	

4.1. SST vs. SL

Sensitivities of prediction errors to magnitudes of the initial SST and SL errors are shown in Figure 8 (upper panels). An evident increase in the prediction error is followed as the initial errors increase. The fact that the doubling of initial errors doubles the error growth points to a quasi-linear relationship between the prediction errors and IC errors. This seems somewhat confusing since we preliminarily thought that there would be a nonlinear relation. In fact, under a long-term (i.e., 12 months) prediction, the model tends to be insensitive to ICs but sensitive to the model itself (revealed in Section 5). In addition, the final SST error growth is dependent on the phase of El Niño. Compared with the onset and decay phase predictions of El Niño, the slope of the error growth is larger in the mature phase prediction.

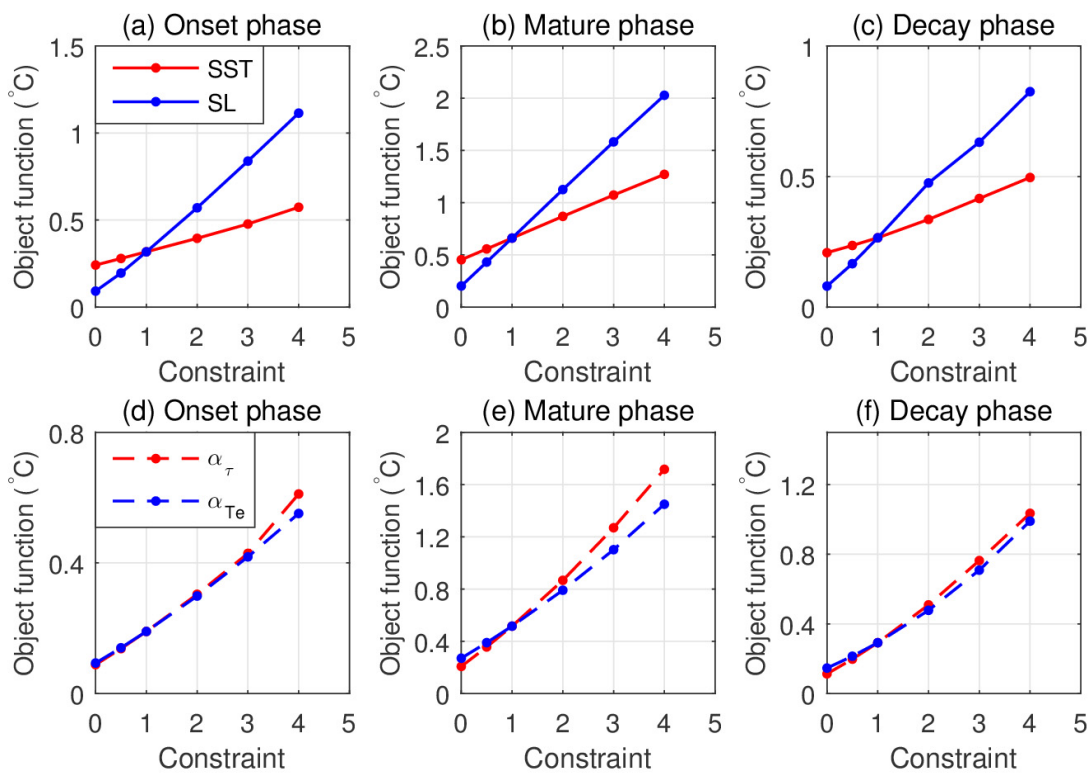


Figure 8. The prediction errors (unit: °C) as the function of constraint for the IC perturbed (a–c) and MP perturbed experiments (d–f) are described in Tables 1 and 2, respectively. The red curves in the upper (bottom) panels denote the cases for initial SST (α_{τ}) perturbed, and blue curves denote cases for initial SL (α_{Te}) perturbed.

The sensitivity of El Niño prediction to uncertainties in individual ICs is different. In comparison with the SST errors, the ICs of the SL errors tend to induce larger uncertainties for the El Niño prediction at any phase. That is, the El Niño prediction is more sensitive to uncertainties in SL than SST. This result supports the study by Zheng et al. (2007) that the prediction uncertainties are reduced by assimilating the observed SL rather than the observed SST [44].

4.2. α_τ vs. α_{Te}

The prediction errors as the function of constraint intensity for MP errors are shown in Figure 8 (bottom panels). It is found that the effort caused by the errors in α_τ and α_{Te} is identical when the constraint is small. However, as the uncertainties associated with MPs grow, errors induced by α_τ become larger than that by α_{Te} , particularly when predicting the mature phase of the El Niño (Figure 8e). Thus, compared with the uncertainties in α_{Te} , the El Niño prediction is more sensitive to the error size in α_τ . That is, the impact of SST-wind feedback on the El Niño prediction is greater than that of SST-thermocline feedback. Another noteworthy observation is the nonlinear relationship between the constraints on MPs and prediction uncertainties. Large errors in MPs can induce an imbalance of the model dynamics so that the error increases rapidly under an unstable prediction. This is supported by evidence that uncertainties in MPs can amplify the uncertainties in predicted wind stress, ultimately resulting in substantial uncertainties in the prediction of ocean dynamics and thermodynamics [7,36].

4.3. ICs vs. MPs

The former experiments have qualitatively examined the sensitivity of the El Niño prediction to the uncertainties in ICs or MPs. The third experiment is finally carried out to compare the impact of ICs and MPs, as well as their combined effect.

Errors induced by the CNOP-I and CNOP-P, as well as CNOPs (i.e., the IC-MP-1, IC-MP-2, and IC-MP-3 experiments), are shown in Figure 9. When both the constraint of ICs and MPs are 1, the errors induced by the CNOP-I and CNOP-P are almost equal. However, as the constraint increases, the CNOP-P causes larger error growth than CNOP-I when predicting the mature and decay phase of the El Niño (Figure 9b,c). This result reflects a plausible fact that the El Niño prediction is more sensitive to uncertainties in MPs.

Another feature that can be found in Figure 9 is that the error induced by CNOPs is much larger than that by CNOP-I or CNOP-P, implying a strong coupling effect between ICs and MPs in El Niño prediction (also shown in Figure 5). Additionally, this combined effect becomes larger along with the intensity of the constraint. For example, the prediction error induced by the CNOPs is lower than 4 °C under the constraint of 2, and the prediction error is larger than 12 °C when the constraint is 4 (Figure 9b). This feature probably contributed to the nonlinear effect caused by the combined effect of IC and MP errors (revealed in Figure 6, in which the nonlinear terms become dominant in error growth).

To elucidate the high combined effect, we conducted a detailed analysis of prediction errors across various regions of the tropical Pacific. The tropical Pacific (15° N–15° S, 140° E–100° W) is divided into nine equal parts (shown in Table 4). We find that the largest error caused is consistently located in the eastern equatorial Pacific in all experiments, hence influencing the prediction of the El Niño intensity. However, as shown in Table 4, the interesting thing is that the CNOPs have the largest combined effect of the equator prediction, where the combined effect can reach 23.5%. This result underscores the critical role of the combined effect of IC and MP errors off the equator in driving the growth of prediction errors.

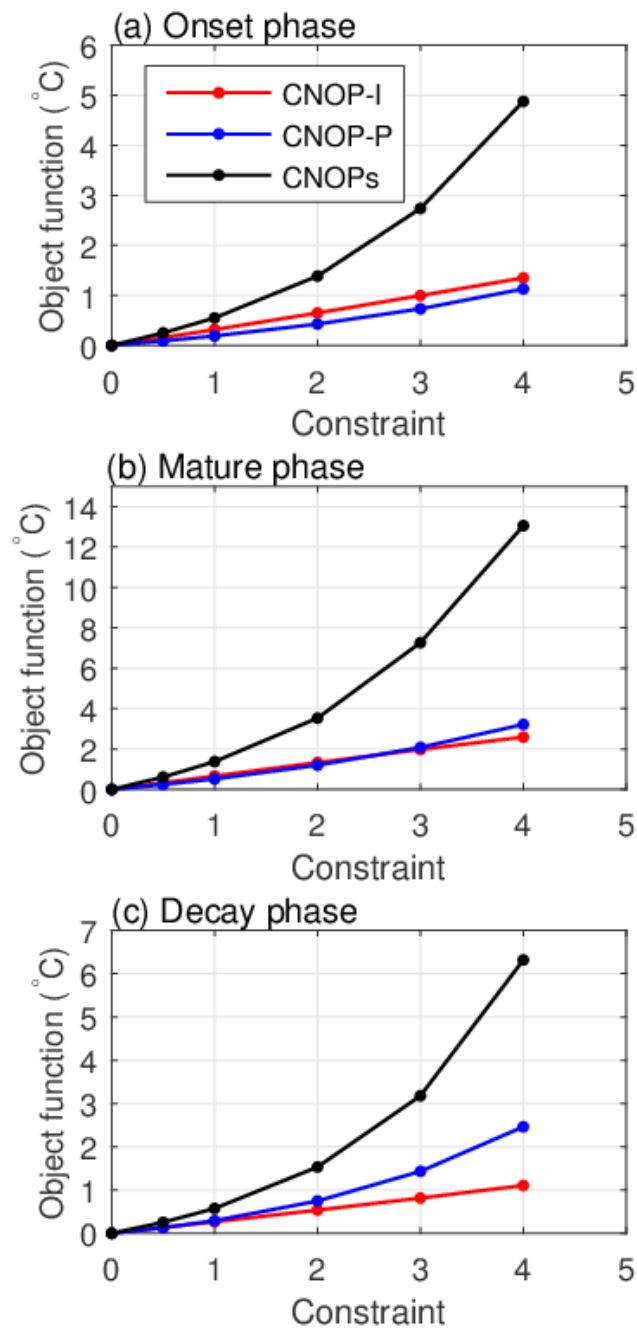


Figure 9. The prediction errors (unit: °C) as the function of constraint that are caused by the CNOP-I (red line), CNOP-P (blue line), and CNOPs (black line) for the (a) onset, (b) mature, and (c) decay phase predictions of El Niño.

Table 4. The combined effect is caused by the errors in the ICs and MPs in the tropical Pacific.

	140°~180° E	180°~140° W	140°~100° W
15° N~5° N	17.3%	19.9%	15.5%
5° N~5° S	14.9%	−2.3%	15.3%
5° S~15° S	5.5%	2.0%	23.5%

5. The Impact of Errors in ICs and MPs Due to Prediction Time

In addition to looking at prediction sensitivity to ICs/MPs, another set of experiments is designed to study the ICs/MPs-induced error growth due to various prediction lengths. CNOP analyses are implemented as standard cases but with diverse prediction lengths. The predictions are carried out with lead times from 3 months to 15 months to predict the onset [June (0)], mature [December (0)], and decay phase [June (1)] of El Niño. The initial times for the predictions are shown in Figure 10. Note that predictions are made on the first day of each selected month.

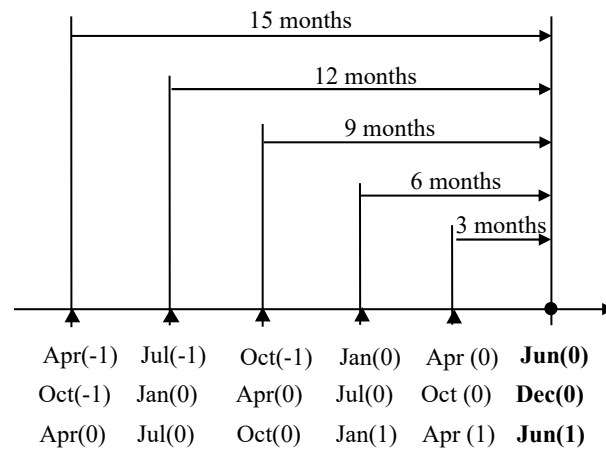


Figure 10. The design of the CNOP analyses with various prediction lengths (i.e., optimization time in the CNOP algorithm) spans from 3 months to 15 months. The filled triangles are the start months, and the solid circles are the final prediction times. Predictions are made on the first day of each month to predict the onset [June (0)], mature [December (0)], and decay phase [June (1)] of the El Niño.

The prediction errors, represented by the object function (i.e., mean RMSE of SST in the tropical Pacific), are presented in Figure 11. Comparing each panel of the figure, it is evident that the relationship between prediction error and prediction length is not related to the El Niño phase. However, such a relationship is dependent on the source of error. Considering the onset phase prediction as an illustrative example (Figure 11a), the prediction errors arising from CNOP-Is fluctuate around 0.3 °C regardless of the prediction length, whereas the errors attributed to MPs gradually increase from 0.1 °C to 0.3 °C. It is indicated that the ICs-induced error starts to saturate at short-term prediction, and the errors induced by the MP errors are still growing as the prediction time increases. This finding aligns with the study conducted by Zheng et al. (2009), who demonstrated that perturbations in ICs have a minimal impact on El Niño predictions, primarily affecting the first three months of the forecast, whereas perturbations in model errors contribute significantly to improving predictions across the entire 12-month period. In practical applications, to achieve accurate predictions, it is crucial to prioritize the accuracy of ICs at shorter lead times (e.g., 3 months) while emphasizing the precision of MPs at longer lead times (e.g., 12 months).

The feature that prediction error is increased with prediction length is evident in CNOP cases where errors in both ICs and MPs are considered. It is found that the interaction of ICs and MPs tends to cause larger prediction errors over time. For example, the error induced by either ICs or MPs is less than 0.3 °C at a 3-month prediction; even at a 12-month leading time, the prediction error is about 0.5 °C (Figure 11b). The error induced by the combination of ICs and MPs intensively increased from 0.4 °C at 3-month prediction to larger than 1.2 °C at 15-month prediction.

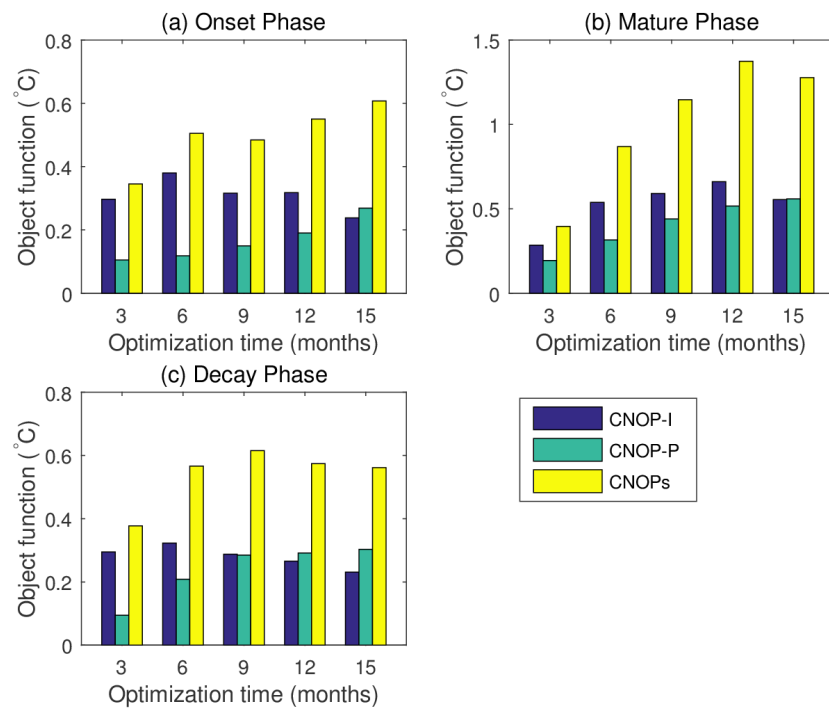


Figure 11. The prediction errors (unit: °C) as the function of the prediction length for the (a) onset, (b) mature, and (c) decay phase predictions of El Niño. The blue, green, and yellow bars are those caused by the CNOP-I, CNOP-P, and CNOPs (i.e., IC-MP-1, IC-MP-2, and IC-MP-3 experiments), respectively.

6. Conclusions and Discussion

Uncertainties in ENSO predictions come from not only ICs but also model dynamics (e.g., the physical processes featured by MPs). In this study, we systematically investigate the impact of errors in ICs and MPs and their combination on El Niño prediction from the optimal error growth perspective. The CNOP approach, which is used to explore the optimal errors in the ICs/MPs that are likely to lead to large error growth in the prediction, is adopted with the ICM. Two ICs (SST and SL) and two MPs (α_τ and α_{T_e}) that are directly related to the Bjerknes positive feedback are considered in the CNOP-I and CNOP-P analysis, respectively. Additionally, the optimally combined error pattern of the MPs and ICs (CNOPs) are calculated in a synchronous manner. The comparison of CNOP-type errors and the corresponding error evolutions allows us to understand the El Niño predictability regarding the two kinds of predictability problems.

Results show that both uncertainties in ICs and MPs have the potential to induce SPB-associated error evolution that presents a rapid error growth in spring, thus deteriorating the prediction of El Niño. However, the underlying processes governing this error growth differ. The spring error growth attributed to CNOP-I is primarily due to uncertainties in ocean advection processes. Conversely, the uncertainties in advection caused by CNOP-P tend to suppress error growth in spring. The spring error growth induced by the MP errors is primarily projected onto uncertainties in thermodynamic processes, encompassing heat flux, diffusion, and conduction. In this light, we should take care of the simulations of the thermodynamics in El Niño prediction when the MPs are not perfect in the ICM, but the simulations of the ocean currents when the ICs are not perfect. Furthermore, the optimally combined mode of the errors in the MPs and the ICs (i.e., CNOPs) produces much larger error growth and causes much more significant SPB. Differing from the CNOP-I and CNOP-P cases, the nonlinear advection terms become dominant in the spring error growth when errors in ICs and MPs are considered simultaneously. This indicates that strong nonlinear interactions exist between the errors in ICs and MPs that aggressively influence the SPB.

The potential impacts of errors in ICs and MPs on the error growth of El Niño predictions across various prediction lengths are demonstrated. It is observed that prediction errors arising from IC errors tend to saturate at short-term prediction horizons (i.e., 3–6 months) as the prediction length increases without a corresponding surge in prediction error. Conversely, errors in MPs tend to induce increasingly larger errors as the prediction time extends. This explains why IC-perturbed ensemble predictions are effective primarily for 3-month forecasts, while model error-perturbed ensemble predictions yield remarkable results at longer lead times [27]. When errors in the ICs and MPs exist simultaneously, the nonlinear interaction between ICs and MPs makes the prediction errors grow much stronger with prediction length than CNOP-I or CNOP-P does. Additionally, the combined nonlinear effect is magnified as the prediction length increases. Consequently, to ensure better prediction accuracy, it is imperative to make concerted efforts to improve both ICs and MPs simultaneously.

The sensitivities of the uncertainties of El Niño prediction to uncertainties in ICs and MPs are revealed. From the CNOP experiments regarding ICs, the El Niño prediction is more sensitive to the information of the SL than the SST. That is, the initial heat content in the tropical is more significant in the prediction of the tropical Pacific. From this point, these results also confirm the previous conclusion that the heat content in the tropical Pacific is a better precursor than the SST to detect the occurrence of the El Niño event [45]. From the CNOP experiments regarding MPs, compared with the uncertainties in α_{Te} , El Niño prediction is more sensitive to uncertainties in α_{τ} . That is, the impact of SST-wind feedback on the El Niño prediction is greater than that of SST-thermocline feedback. Moreover, the relative importance of ICs and MPs in El Niño prediction is investigated with the conclusion that the El Niño prediction is more sensitive to uncertainties in MPs than that in ICs. Hence, we suggest a priority of improvement in MPs or the model itself so as to give a better prediction when computing resources are limited, especially for the state-of-the-art models.

We are not denying the effectiveness of the data assimilations that balance the ICs and model. On the contrary, we emphasize that the initial and model errors should be simultaneously considered for greatly improving the El Niño prediction level [35] since the nonlinear interactions between the errors that existed in ICs and MPs make El Niño difficult to predict. We also acknowledge the limitations of the present study, such as the simplified model adopted. More relevant studies are expected to be conducted. For example, how can an effective scheme to improve the prediction except for the target observation be designed [24]? An alternative approach is to obtain the optimal model errors based on the observations and model rather than subjectively or empirically [37,41,46,47]. For example, as demonstrated by Zhang et al. (2018), the optimized MPs and ICs are obtained based on the CNOP approach, which is then used to successfully predict the 2015 El Niño event [13]. In spite of all this, this study deepens our understanding of El Niño predictability.

Funding: This study was supported by the Ministry of Science and Technology of the People's Republic of China (Grant No. 2020YFA0608802) and the Startup Foundation for Introducing Talent of NUIST.

Institutional Review Board Statement: Not applicable.

Informed Consent Statement: Not applicable.

Data Availability Statement: The datasets generated by the ICM and CNOP approach are not publicly available due to the large size of data but are available from the corresponding author upon reasonable request. All scripts used to analyze the data and generate the figures have been written using the Grads language and MATLAB.

Acknowledgments: I would like to express my sincere gratitude to two anonymous reviewers. Also, I would like to express my deepest gratitude to Ronghua Zhang, Mu Mu, and Wansuo Duan for their instructive comments and suggestions.

Conflicts of Interest: The authors have no relevant financial or non-financial interests to disclose.

References

- McPhaden, M.J.; Zebiak, S.E.; Glantz, M.H. ENSO as an integrating concept in Earth science. *Science* **2006**, *314*, 1740–1745. [[CrossRef](#)] [[PubMed](#)]
- Alexander, M.A.; Blade, I.; Newman, M.; Lanzante, J.R.; Lau, N.C.; Scott, J.D. The atmospheric bridge: The influence of ENSO teleconnections on air-sea interaction over the global oceans. *J. Clim.* **2002**, *15*, 2205–2231. [[CrossRef](#)]
- Xie, S.P.; Deser, C.; Vecchi, G.A.; Ma, J.; Teng, H.Y.; Wittenberg, A.T. Global Warming Pattern Formation: Sea Surface Temperature and Rainfall. *J. Clim.* **2010**, *23*, 966–986. [[CrossRef](#)]
- Andersen, L.K.; Davis, M.D.P. The effects of the El Niño Southern Oscillation on skin and skin-related diseases: A message from the International Society of Dermatology Climate Change Task Force. *Int. J. Dermatol.* **2015**, *54*, 1343–1351. [[CrossRef](#)]
- Ashok, K.; Behera, S.K.; Rao, S.A.; Weng, H.Y.; Yamagata, T. El Niño Modoki and its possible teleconnection. *J. Geophys. Res.-Ocean.* **2007**, *112*. [[CrossRef](#)]
- Capotondi, A.; Wittenberg, A.T.; Newman, M.; Di Lorenzo, E.; Yu, J.Y.; Braconnot, P.; Cole, J.; Dewitte, B.; Giese, B.; Guilyardi, E.; et al. Understanding ENSO Diversity. *Bull. Am. Meteorol. Soc.* **2015**, *96*, 921–938. [[CrossRef](#)]
- Zebiak, S.E.; Cane, M.A. A Model El-Niño Southern Oscillation. *Mon. Weather Rev.* **1987**, *115*, 2262–2278. [[CrossRef](#)]
- Chen, D.; Zebiak, S.E.; Busalacchi, A.J.; Cane, M.A. An Improved Procedure for El Niño Forecasting: Implications for Predictability. *Science* **1995**, *269*, 1699–1702. [[CrossRef](#)] [[PubMed](#)]
- McPhaden, M.J.; Busalacchi, A.J.; Cheney, R.; Donguy, J.R.; Gage, K.S.; Halpern, D.; Ji, M.; Julian, P.; Meyers, G.; Mitchum, G.T.; et al. The tropical ocean global atmosphere observing system: A decade of progress. *J. Geophys. Res.-Ocean.* **1998**, *103*, 14169–14240. [[CrossRef](#)]
- Ham, Y.G.; Kug, J.S. Improvement of ENSO Simulation Based on Intermodel Diversity. *J. Clim.* **2015**, *28*, 998–1015. [[CrossRef](#)]
- Zhang, R.H.; Gao, C.; Feng, L.C. Recent ENSO evolution and its real-time prediction challenges. *Natl. Sci. Rev.* **2022**, *9*, nwac052. [[CrossRef](#)]
- Min, Q.Y.; Su, J.Z.; Zhang, R.H.; Rong, X.Y. What hindered the El Niño pattern in 2014? *Geophys. Res. Lett.* **2015**, *42*, 6762–6770. [[CrossRef](#)]
- Zhang, R.H.; Tao, L.J.; Gao, C. An improved simulation of the 2015 El Nio event by optimally correcting the initial conditions and model parameters in an intermediate coupled model. *Clim. Dyn.* **2018**, *51*, 269–282. [[CrossRef](#)]
- Chen, D.; Lian, T. Effects of westerly wind bursts on El Nio: A new perspective. *Geophys. Res. Lett.* **2014**, *41*, 3522–3527. [[CrossRef](#)]
- Ji, C.P.; Mu, M.; Fang, X.H.; Tao, L.J. Improving the Forecasting of El Niño Amplitude Based on an Ensemble Forecast Strategy for Westerly Wind Bursts. *J. Clim.* **2023**, *36*, 8675–8694. [[CrossRef](#)]
- Lorenz, E.N. Climatic predictability in the physical basis of climate and climate modeling. *WMO GARP Publ. Ser No* **1975**, *16*, 132–136.
- Mu, M.; Duan, W.S.; Chou, J.F. Recent advances in predictability studies in China (1999–2002). *Adv. Atmos. Sci.* **2004**, *21*, 437–443. [[CrossRef](#)]
- Mu, M.; Duan, W.; Wang, Q.; Zhang, R. An extension of conditional nonlinear optimal perturbation approach and its applications. *Nonlinear Process. Geoph.* **2010**, *17*, 211–220. [[CrossRef](#)]
- Xue, Y.; Cane, M.A.; Zebiak, S.E. Predictability of a coupled model of ENSO using singular vector analysis. 1. Optimal growth in seasonal background and ENSO cycles. *Mon. Weather Rev.* **1997**, *125*, 2043–2056. [[CrossRef](#)]
- Tang, Y.M.; Kleeman, R.; Miller, S. ENSO predictability of a fully coupled GCM model using singular vector analysis. *J. Clim.* **2006**, *19*, 3361–3377. [[CrossRef](#)]
- Mu, M.; Duan, W.S.; Wang, B. Conditional nonlinear optimal perturbation and its applications. *Nonlinear Process. Geoph.* **2003**, *10*, 493–501. [[CrossRef](#)]
- Mu, M.; Duan, W.S.; Tang, Y.M. The predictability of atmospheric and oceanic motions: Retrospect and prospects. *Sci. China Earth Sci.* **2017**, *60*, 2001–2012. [[CrossRef](#)]
- Webster, P.J. The Annual Cycle and the Predictability of the Tropical Coupled Ocean-Atmosphere System. *Meteorol. Atmos. Phys.* **1995**, *56*, 33–55. [[CrossRef](#)]
- Mu, M.; Duan, W.S.; Chen, D.K.; Yu, W.D. Target observations for improving initialization of high-impact ocean-atmospheric environmental events forecasting. *Natl. Sci. Rev.* **2015**, *2*, 226–236. [[CrossRef](#)]
- Duan, W.S.; Huo, Z.H. An Approach to Generating Mutually Independent Initial Perturbations for Ensemble Forecasts: Orthogonal Conditional Nonlinear Optimal Perturbations. *J. Atmos. Sci.* **2016**, *73*, 997–1014. [[CrossRef](#)]
- Duan, W.S.; Zhao, P.; Hu, J.Y.; Xu, H. The Role of Nonlinear Forcing Singular Vector Tendency Error in Causing the “Spring Predictability Barrier” for ENSO. *J. Meteorol. Res.* **2016**, *30*, 853–866. [[CrossRef](#)]
- Zheng, F.; Wang, H.; Zhu, J. ENSO ensemble prediction: Initial error perturbations vs. model error perturbations. *Chin. Sci. Bull.* **2009**, *54*, 2516–2523. [[CrossRef](#)]
- Qi, Q.Q.; Duan, W.S.; Zheng, F.; Tang, Y.M. On the “spring predictability barrier” for strong El Nio events as derived from an intermediate coupled model ensemble prediction system. *Sci. China Earth Sci.* **2017**, *60*, 1614–1631. [[CrossRef](#)]
- Liu, Z.Y. A simple model study of ENSO suppression by external periodic forcing. *J. Clim.* **2002**, *15*, 1088–1098. [[CrossRef](#)]
- Macmynowski, D.G.; Tziperman, E. Factors affecting ENSO’s period. *J. Atmos. Sci.* **2008**, *65*, 1570–1586. [[CrossRef](#)]
- Gao, C.; Zhang, R.H. The roles of atmospheric wind and entrained water temperature (T-e) in the second-year cooling of the 2010–12 La Nina event. *Clim. Dyn.* **2017**, *48*, 597–617. [[CrossRef](#)]

32. Zhang, R.H.; Zheng, F.; Zhu, J.; Wang, Z.G. A successful real-time forecast of the 2010-11 La Nina event. *Sci. Rep.* **2013**, *3*, 1108. [[CrossRef](#)]
33. Duan, W.S.; Zhang, R. Is model parameter error related to a significant spring predictability barrier for El Nio events? Results from a theoretical model. *Adv. Atmos. Sci.* **2010**, *27*, 1003–1013. [[CrossRef](#)]
34. Yu, Y.S.; Mu, M.; Duan, W.S. Does Model Parameter Error Cause a Significant “Spring Predictability Barrier” for El Niño Events in the Zebiak-Cane Model? *J. Clim.* **2012**, *25*, 1263–1277. [[CrossRef](#)]
35. Wu, X.R.; Han, G.J.; Zhang, S.Q.; Liu, Z.Y. A study of the impact of parameter optimization on ENSO predictability with an intermediate coupled model. *Clim. Dyn.* **2016**, *46*, 711–727. [[CrossRef](#)]
36. Tao, L.J.; Gao, C.; Zhang, R.H. Model parameter-related optimal perturbations and their contributions to El Niño prediction errors. *Clim. Dyn.* **2019**, *52*, 1425–1441. [[CrossRef](#)]
37. Zhang, R.H.; Zebiak, S.E.; Kleeman, R.; Keenlyside, N. A new intermediate coupled model for El Niño simulation and prediction. *Geophys. Res. Lett.* **2003**, *30*. [[CrossRef](#)]
38. Zhang, R.H.; Zebiak, S.E.; Kleeman, R.; Keenlyside, N. Retrospective El Niño forecasts using an improved intermediate coupled model. *Mon. Weather. Rev.* **2005**, *133*, 2777–2802. [[CrossRef](#)]
39. Gao, C.; Wu, X.R.; Zhang, R.H. Testing a four-dimensional variational data assimilation method using an improved intermediate coupled model for ENSO analysis and prediction. *Adv. Atmos. Sci.* **2016**, *33*, 875–888. [[CrossRef](#)]
40. Tao, L.J.; Zhang, R.H.; Gao, C. Initial error-induced optimal perturbations in ENSO predictions, as derived from an intermediate coupled model. *Adv. Atmos. Sci.* **2017**, *34*, 791–803. [[CrossRef](#)]
41. Tao, L.J.; Duan, W.S. Using a nonlinear forcing singular vector approach to reduce model error effects in ENSO forecasting. *Weather Forecast.* **2019**, *34*, 1321–1342. [[CrossRef](#)]
42. Xu, K.; Huang, R.X.; Wang, W.Q.; Zhu, C.W.; Lu, R.Y. Thermocline Fluctuations in the Equatorial Pacific Related to the Two Types of El Niño Events. *J. Clim.* **2017**, *30*, 6611–6627. [[CrossRef](#)]
43. Bjerknes, J. Atmospheric Teleconnections from Equatorial Pacific. *Mon. Weather Rev.* **1969**, *97*, 163–172. [[CrossRef](#)]
44. Zheng, F.; Zhu, J.; Zhang, R.H. Impact of altimetry data on ENSO ensemble initializations and predictions. *Geophys. Res. Lett.* **2007**, *34*, 256–260. [[CrossRef](#)]
45. Duan, W.S.; Hu, J.Y. The initial errors that induce a significant “spring predictability barrier” for El Niño events and their implications for target observation: Results from an earth system model. *Clim. Dyn.* **2016**, *46*, 3599–3615. [[CrossRef](#)]
46. Zhu, Y.C.; Zhang, R.H. An Argo-Derived Background Diffusivity Parameterization for Improved Ocean Simulations in the Tropical Pacific. *Geophys. Res. Lett.* **2018**, *45*, 1509–1517. [[CrossRef](#)]
47. Tao, L.J.; Duan, W.S.; Vannitsem, S. Improving forecasts of El Niño diversity: A nonlinear forcing singular vector approach. *Clim. Dyn.* **2020**, *55*, 739–754. [[CrossRef](#)]

Disclaimer/Publisher’s Note: The statements, opinions and data contained in all publications are solely those of the individual author(s) and contributor(s) and not of MDPI and/or the editor(s). MDPI and/or the editor(s) disclaim responsibility for any injury to people or property resulting from any ideas, methods, instructions or products referred to in the content.